American Journal of Applied Sciences

Research Article

Comparative Analysis of Five Decomposition Techniques for Monthly Rainfall Time Series from 1991 to 2020 in Guinea (West Africa)

Noukpo Médard Agbazo[1], Oumar Keita[1], Alpha Oumar Baldé[2], Lonsenigbè Camara[1] and Lancei Koivogui[1]

[1]*Département d'Hydrologie, Université de N'zérékoré, 50 BP, N'zérékoré, Guinea*
[2]*Département de Mathématiques, Université de N'zérékoré, 50 BP, N'zérékoré, Guinea*

Article history
Received: 07-06-2025
Revised: 08-08-2025
Accepted: 04-09-2025

Corresponding Author:
Noukpo Médard Agbazo
Département d'Hydrologie, Université de N'zérékoré, Guinea
Email: agbmednou@gmail.com

Abstract: The selection of an optimal time series decomposition' technique is crucial for enhancing rainfall prediction by using sophisticated methods as deep learning hybrid approaches. This study evaluates the effectiveness of five times series decomposition techniques in analyzing monthly rainfall datasets across Guinea geographical regions (Lower-Guinea (Boké, Conakry, Kindia), Middle-Guinea (Labé, Mamou), Upper-Guinea (Faranah, Kankan) and Forest-Guinea (Nzérékoré)) and identifies the most suitable technique for each region. The decomposition techniques considered are (a) Variational Mode Decomposition (VMD), (b) Ensemble Empirical Mode Decomposition (EEMD), (c) Complete Ensemble Empirical Mode Decomposition (CEEMD), (d) Complete Ensemble Empirical Mode Decomposition Adaptive Noise (CEEMDAN) and (e) Improved Complete EEMD with Adaptive Noise (ICEEMDAN) techniques. These techniques were chosen due to their widespread use and high accuracy. Their performance was judged using Kolmogorov-Smirnov Statistic (DKS), Root Mean Square Error (RMSE), Mean Square Error (MSE) and Mean Absolute Error (MAE). The results demonstrate that ICEEMDAN and CEEMDAN techniques showed the lowest RMSE, MAE, and MSE values compared to the others ones at all of the studied sites, indicating highest decomposition performances. However, ICEEMDAN consistently exhibited smaller DKS values compared to CEEMDAN, except in the site of Faranah and Nzérékoré. Therefore, ICEEMDAN is recommended as the most suitable technique for most studied stations, while CEEMDAN is preferable for Faranah and Nzérékoré. The analysis also revealed that monthly rainfall trends during the study period were predominantly nonlinear across all the sites. These nonlinear trends exhibited complex patterns such as alternating increases, suggesting significant climatic shift around the 2010s. The results highlight the limitations of traditional methods that assume linearity in rainfall trend detection, which may yield inaccurate conclusions. The finding provides valuable insights for improving rainfall forecasting in Guinea and enhancing our understanding of rainfall temporal variations in the period from 1991 to 2020.

Keywords: Rainfall, Guinea, Decomposition, VMD, EEMD, CEEMD, CEEMDAN, ICEEMDAN

Introduction

Rainfall time series forecasting is crucial for managing and planning water reserves and improving agricultural productivity (Wani *et al*., 2024; Zhou *et al*., 2021; Xu *et al*., 2022). Unfortunately, rainfall prediction is a complex and challenging task due to the intrinsic characteristics of rainfall, such as its extreme variability, greater randomness and multiscale properties (Jiao and He, 2024; Agbazo *et al*., 2023; Yang *et al*., 2024; Ling *et al*., 2023).

Therefore, enhancing the precision of rainfall forecasting has been a main domain of research (Zhang *et al*., 2025), mainly in countries characterized by different climatic regions and affected by changing climate.

Nowadays, performing rainfall predicting with Machine Learning (ML) and Deep Learning (DL) algorithms has received particular attention by researchers world-wide (Ali *et al*., 2020; Wani *et al*., 2024; Wang *et al*., 2021; Huang *et al*., 2022), but not yet spread in Guinea (West Africa). These techniques have revealed notable potential in rainfall forecasting (Zhang *et al*., 2025; Poongadan and Lineesh, 2024; Ali *et al*., 2020; Adarsh and Reddy, 2018; 2021). However, due to the intrinsic physical mechanisms characterizing rainfall, these algorithms present certain limitations in rainfall forecasting, affecting considerably forecasting accuracy (Sánchez-Monedero *et al*., 2014; Ali *et al*., 2018). Indeed, it is argued in many literatures, that due to the nonlinearity, nonstationarity and multiscale properties of rainfall time series, the accuracy of forecasting is greatly reduced when individual ML or DL algorithms are used (Huang *et al*., 2022; Sánchez-Monedero *et al*., 2014). Due to the naturally occurring nonlinearity, nonstationarity, and multiscale properties inherent in rainfall time series, achieving high forecasting accuracy using only a Machine Learning (ML) or Deep Learning (DL) algorithm is challenging (Huang *et al*. 2022; Sánchez-Monedero *et al*., 2014; Adarsh and Reddy, 2018; 2021).

To enhance the reliability of rainfall forecasting, it is necessary to approach the challenges of nonstationarity and nonlinearity challenges faced by ML and DL forecasting algorithms (Adarsh and Reddy, 2021). To this end, numerous studies have recommended the use of the decomposition-based hybrid models which, by coupling ML or DL algorithm, can significantly improve rainfall forecasting accuracy (Adarsh and Reddy, 2018; 2021; Khan *et al*., 2020; Danandeh, 2021).

In literature, the commonly used decomposition techniques for breaking down rainfall data into a series of periodic terms and components before applying ML and DL algorithms include Wavelet Analysis (WA) (Pati *et al*., 1993); EMD (Huang *et al*., 1998); EEMD (Wu *et al*., 2009c); CEEMD (Torres *et al*., 2011); CEEMDAN (Torres *et al*., 2011; Colominas *et al*., 2012); ICEEMDAN (Colominas *et al*., 2014) and VMD (Dragomiretskiy and Zosso, 2014; Zhang *et al*., 2023). Among the aforementioned techniques, the WA approach is less effective and has received less attention in rainfall forecast studies because the mother wavelets and decomposition level should be predetermined before (Wu *et al*., 2009a-b; Rezaiy and Shabri, 2024). Moreover, WA technique is more suitable for nonstationary and linear data processing (Wu *et al*., 2009a-b).

Several authors have combined decomposition-based hybrid models to enhance rainfall forecasting. Notable examples include: The combination of Wavelet Analysis (WA) and Artificial Neural Network (ANN) (Adamowski and Sun, 2010; Seo *et al*., 2015); EMD or VMD with long Short-Term Memory (LSTM) (Huang *et al*., 2022); CEEMD and Random Forest (RF) (Ali *et al*., 2020); CEEMD and LSTM (Jiang, 2023); EEMD and LSTM (Yang *et al*., 2021); EEMD and ANN (Johny *et al*., 2020); EMD and ANN (Iyengar and Raghu, 2005; Tan *et al*., 2018) ; CEEMDAN and bi-directional long Short-term memory neural network (BiLSTM) (Zhang *et al*., 2023); VMD and BiLSTM (Jiao and He, 2024); ICEEMDAN and LSTM (Yang *et al*., 2024; Poongadan and Lineesh 2024); CEEMDAN and Extreme Learning Machine (ELM) (Zhang *et al*., 2022); ICEEMDAN and ANN (Johny *et al*., 2020), among others. The results of these studies indicate that coupling ML or DL algorithm with data decomposition techniques significantly improve rainfall time series forecasting compared to using ML or DL algorithms alone. However, the performance and predictive capabilities of these hybrid models are thoroughly relying on the effectiveness of the chosen time series decomposition technique, which varies based on climatic conditions and geographical regions. Therefore, selecting the most suitable decomposition technique is crucial for enhancing rainfall forecasting accuracy with ML and DL algorithms.

Guinea Republic is a country in West Africa, characterized by four geographical regions and is significantly affected by climate change effects. Agriculture, which is predominantly rainfed and accounts for approximately 22 % of the national GDP and serves as a primary economic activity for 70 % of Guineans (USAID, 2018). There was a gap in research conducted previously in Guinea using hybrid models for rainfall forecasting. Additionally, there is a deficiency of research investigating on time series decomposition techniques across the country's different geographical regions. Given that, the choice of the best time series decomposition techniques in each geographical region is crucial for improving rainfall forecasting. There is a pressing need for studies comparing the effectiveness of time series decomposition techniques across Guinea geographical regions. Therefore, this preliminary study aims to measure and compare the achievement of VMD, EEMD, CEEMD, CEEMDAN and ICEEMDAN techniques to identify the most effective technique for each administrative region of Guinea.

Materials

Study Area Description

Guinea is situated in West Africa, between 7˚N and 13˚N as latitudes, and 7˚W and 15˚W longitudes (Figure 1a). The country predominantly experiences a tropical climate, with annual temperature ranging between 23°C and 29°C. The total amount of annual rainfall varies between 1,500 and 4,500 mm, following a pronounced south-to-north gradient: Decreasing from south and along the coast to the north and inland areas (Guinea, 2018;

USAID, 2018). Most of Guinea regions experience two distinct seasons per year: A long rainy season, from April to November, and a dry season from December to March (Guinea, 2018; USAID, 2018; World Bank, 2016; 2017). The country is subdivided into four geographical regions:

1. The Lower-Guinea (LG) in the coastal region, characterized by greater temperature includes the stations of Boké, Conakry and Kindia
2. The Middle-Guinea (MG), characterized by the Fouta Djallon highlands, it encompasses the stations of Labé and Mamou
3. The Upper-Guinea (UG) situated in the north of the country includes stations in Faranah and Kankan
4. The Forest-Guinea (FG) located in the southeastern part of Guinea, includes the station of Nzérékoré

The climate at the Upper Guinea is similar to Sahelian climate, with greater temperature ranges and a longer dry season (December-May), and annual rainfall ranging between 1.200 mm in the north to 1.600 mm in the south. In contrast, the coastal and southern (or forest) regions of Guinea has a monsoon climate with a shorter dry season and are typified by a lengthy rainy season (seven to nine months) and smaller temperature variations than the interior (Kante *et al*., 2020; 2019; Guinea, 2018; USAID, 2018; World Bank, 2016; 2017).

Data Description

For this study, monthly rainfall time series for the 1991-2020 period were used. The dataset was provided by the Guinean National Meteorological Service and they were obtained from eight synoptic stations distributed across Guinea (Figure 1b).

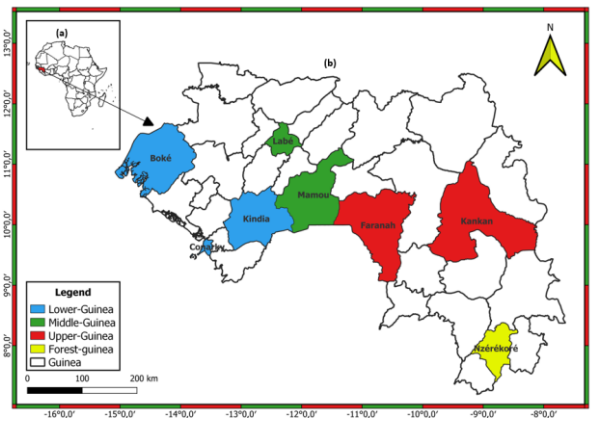

Fig. 1: (a) Map Illustrating the Guinea's Geographic Location within Africa. (b) Geographical cities to the East, West, North and South of the overall regional boundary of study area. These geographical cities are classified into four geophysical regions as follows: Lower-Guinea (Boké, Conakry, Kindia), Middle-Guinea (Labé,Mamou), Upper-Guinea (Faranah, Kankan) and Forest-Guinea (Nzérékoré)

Table 1 shows statistics of rainfall for the studied synoptic stations. From this table it can be noted that during the studied period: The mean (maximum) rainfall is weakest for Kankan (Nzérékoré) and highest for Conakry (Conakry). The standard deviatsion is weakest for Nzérékoré and highest for Conakry. The skewness is positive for all stations, however, the highest skewness is observed for Faranah, while the lowest is for Nzérékoré. These findings indicate that Nzérékoré experiences a more symmetrical rainfall distribution with moderate and consistent patterns, whereas Faranah exhibits an asymmetric distribution with a tendency toward more extreme rainfall variations. The kurtosis values for Boké, Conakry, Faranah and Kankan are greater than 3, indicating that their distributions are leptokurtic. However, stations at Mamou, Kindia, Labé, Nzérékoré have kurtosis values less than 3, meaning, their distributions are platykurtic. The smallest kurtosis value is observed for Kindia, while the largest is Faranah. Overall, mean rainfall values arranging from 121 to 311 mm exemplify the substantial diversity in rainfall levels over Guinea.

Methods

Ensemble Empirical Mode Decomposition (EEMD) Algorithm

For a given observed series *y(t),* the EEMD steps are as follows (Wu, 2009):

Step 1: Generate a new rainfall dataset $x_i(t)$:

$$x_i(t) = y(t) + \eta_i(t), \mathrm{i} = 1, 2, \ldots, m \quad (1)$$

Where $\eta_i(t)$ is a Gaussian white noise (zero-mean unit-variance white Gaussian noise) and m (usually set at 1,000) is the number of realizations of Gaussian white noise:

Step 2: Use EMD algorithm (Huang *et al*., 1998) to completely decompose each $x_i(t)$:

$$x_i(t) = \sum_{k=1}^{n} IMF_{ik}(t) + r_i(t) \quad (2)$$

Table 1: Descriptive Statistics of the Study Synoptic Stations

Study stations	Climatological statistics (1991-2020)				
	Mean (mm)	Max (mm)	Std (mm)	Skew (mm)	Kurt (mm)
Boké	192.24	1168.00	234.28	1.08	3.66
Conakry	310.82	1677.00	422.04	1.40	3.90
Kindia	168.87	636.30	175.82	0.74	2.41
Labé	131.55	635.00	143.82	0.88	2.88
Mamou	147.70	729.30	153.54	0.86	2.98
Faranah	136.97	1528.30	167.27	3.03	22.03
Kankan	120.92	612.500	134.94	1.10	3.63
Nzérékoré	158.26	539.60	116.84	0.50	2.62

Where $IMF_{ik}(t)$ and $r_i(t)$ denote the i^{th} Intrinsic Mode Function (IMF) component and residue from $x_i(t)$ the EMD technique. Where *n* indicates the number of IMF:

Step 3: Finally, take the ensemble average of IMFs components and residue obtained from $x_i(t)$ with EMD technique:

$$\overline{IMF}_k = \frac{1}{m}\sum_{i=1}^{m} IMF_{ik}(t) \text{ and } R(t) = \frac{1}{m}\sum_{i}^{m} r_i(t) \quad (3)$$

Where $\overline{IMF}_k(t)$ and $R(t)$ are respectively the k^{th} mode and residue (nonlinear trend) of *y(t)*. Thus, the observed series is formulated as:

$$y(t) = \sum_{k=1}^{n} \overline{IMF}_k(t) + R(t) \quad (4)$$

Complete Ensemble Empirical Mode Decomposition (CEEMD) Algorithm

According to Li *et al*. (2023); Ali *et al*. (2020); Torres *et al*. (2011), for a given observed rainfall sets y(t), the computation steps of CEEMD are:

Step 1: Deduce the first decomposed component applying EMD to (*y*(*t*) + white noise)
Step 2: Rehearse the decomposition and append white noise of different realizations
Step 3: Calculate the ensemble mean to establish the first IMF_1:

$$IMF_1(t) = \frac{1}{N}\sum_{i=1}^{N} E_1[y(t) + \sigma w_i] \quad (5)$$

Where σ is a ratio coefficient, *N* is the realizations' number, $w_i(t)$ denotes the different white noise, and E_1 represents generating i^{th} *IMF* component:

Step 4: Compute the prime residue:

$$r_1(t) = y(t) - IMF_1(t) \quad (6)$$

Step 5: Compute the second *IMF* component IMF_2:

$$IMF_2(t) = \frac{1}{N}\sum_{i=1}^{N} E_1(r_1(t) + \sigma E_1[w_i(t)]) \quad (7)$$

Step 6: Replicate the aforementioned steps to get the $(n+1)^{th}$ *IMF* component, $IMF_{n+1}(t)$:

$$IMF_{n+1}(t) = \frac{1}{N}\sum_{i=1}^{N} E_1(r_n(t) + \sigma E_n[w_i(t)]) \quad (8)$$

$$y(t) = \sum_{i=1}^{N} IMF_i(t) + R(t) \quad (9)$$

IMF_i and $R(t)$ are respectively the i^{th} mode and residue (nonlinear trend) of *y(t)*.

Complete EEMD With Adaptive Noise (CEEMDAN) Algorithm

According to (Torres *et al*., 2011; Colominas *et al*., 2012; Antico *et al*., 2014) for a given observed rainfall sets y(t), the computation steps of CEEMDAN are:

Step 1: Produce a new rainfall set $x_i(t)$:

$$x_i(t) = y(t) + \beta_0\eta_i(t) \quad (10)$$

Where $\eta_i(t)$ is the white Gaussian noise realization (*i = 1, 2, ..., m*) with the unit-variance and zero-mean; β_0 ($\beta_0 > 0$) represents the noise level:

Step 2: Decompose entirely $x_i(t)$ *m* times through the EMD technique to get the first intrinsic mode function $IMF_{i1}(t)$ (*i=1, 2, ..., m*) and determine the first *IMF* of CEEMDAN and the initial residual $R_1(t)$ as follows:

$$\overline{IMF}_1 = \frac{1}{m}\sum_{i=1}^{m} IMF_{i1}(t) \quad (11)$$

$$R_1(t) = y(t) - \overline{IMF}_1(t) \quad (12)$$

Step 3: Generate a new rainfall set $R_{i1}(t)$:

$$R_{i1}(t) = R_1(t) + \beta_1 E_1(\eta_i(t)) \quad (13)$$

Where the operator $E_k(\cdot)$ denotes the k^{th} *IMF* decomposed by EMD:

Step 4: Decompose $R_{i1}(t)$ 1 times through the EMD technique to get the second IMF ($\overline{IMF}_2$) of CEEMDAN and the initial residual $R_2(t)$ as follows:

$$\overline{IMF}_2 = \frac{1}{m}\sum_{i=1}^{m} E_1(R_1(t) + \beta_1 E_1(\eta_i(t))) \quad (14)$$

$$R_2(t) = R_1(t) - \overline{IMF}_2(t) \quad (15)$$

Step 5: Replicate Step 3 and 4, therefore, the *k-th* (*k = 2, 3, ..., n*) *IMF* and residual are summarized as:

$$\overline{IMF}_k = \frac{1}{m}\sum_{i=1}^{m} E_1(R_{k-1}(t) + \beta_{k-1}E_{k-1}(\eta_i(t))) \quad (16)$$

$$R_k(t) = R_{k-1}(t) - \overline{IMF}_k(t) \quad (17)$$

Where β_k is the level of added white noise. The value of β_k vary usually between 0.1 and 0.3 (Colominas *et al*. 2012):

Step 6: Eventually, move to Step 5 for the next *k* up to the obtained residual cannot continue the decomposition by EMD. At that time, the ultimate residue satisfies the following equation:

$$R(t) = y(t) - \sum_k^n \overline{IMF}_k\,(t) \tag{18}$$

n is the entire number of modes. Therefore, the observed series *y(t)* can be written as:

$$y(t) = \sum_k^n \overline{IMF}_k\,(t) + R(t) \tag{19}$$

Where $\overline{IMF}_k(t)$ and $R\,(\mathrm{t})$ represent respectively the different periodic characteristics and the nonlinear trend.

Improved Complete EEMD WITH Adaptive Noise (ICEEMDAN) Algorithm

According to Colominas *et al*. (2014) for a given observed rainfall sets *y(t),* the computation steps of ICEEMDAN are:

Step 1: Produce a new rainfall set $x_i(t)$:

$$x_i(t) = y(t) + \beta_0 E_1(\eta_i(t) \tag{20}$$

Where $\eta_i(t)$ denotes the ith white Gaussian noise added:

Step 2: Decompose completely $x_i(t)$ m times with EMD technique to get IMF_1 of the improved CEEMDAN:

$$R_1(t) = \frac{1}{m}\sum_{i=1}^m M\big(x_i(t)\big) \tag{21}$$

$$\widetilde{IMF}_1(t) = y(t) - R_1(t) \tag{22}$$

Step 3: Determine IMF_2 and residual of the improved CEEMDAN as follows:

$$\widetilde{IMF}_2(t) = R_1(t) - R_2(t) \tag{23}$$

$$R_2(t) = \frac{1}{m}\sum_{i=1}^m M(R_1(t) + \beta_1 E_2(\eta_i(t))) \tag{24}$$

Step 4: Determine IMF_k of the improved CEEMDAN:

$$\widetilde{IMF}_k(t) = R_{k-1}(t) - R_k(t) \tag{25}$$

$$R_k(t) = \frac{1}{m}\sum_{i=1}^m M(R_{k-1}(t) + \beta_{k-1} E_k(\eta_i(t))) \tag{26}$$

Step 5: Eventually, move to Step 4 for the next *k*, up to the turn off criterion is attained

Thus, *y(t)* can be expressed as:

$$y(t) = \sum_k^n \widetilde{IMF}_k\,(t) + R(t) \tag{27}$$

$R(t)$ is the real nonlinear trend.

In this study, m = 1000, and $\beta_k = 0.2$ in order to compare EEMD, CEEMD, ICEEMDAN and CEEMDAN results.

Variational Mode Decomposition (VMD)

According to Dragomiretskiy and Zosso (2014) for a given observed rainfall sets *y*(*t*), the computation steps of VMD are:

Step 1: Constructing a variational problem as follows:

$$\begin{cases} \min\limits_{\{u_k\},\{\omega_k\}} \left\{\sum_k^K \left\| \partial_t \left[\left(\delta(t) + \frac{j}{\pi t}\right) * u_k(t)\right] e^{-jw_k^t}\right\|_2^2\right\} \\ \sum_{k=1}^K u_k\,(t) = y(t) \end{cases} \tag{28}$$

Where: $j = \sqrt{-1}$; δ is Dirac distribution; $*$ denotes convolution operator; $y(t)$ denotes sum of the components of input series; K is the number of IMFs; $\{u_k(t)\} := \{u_1, u_2, \cdots, u_n\}$ the set of all modes ; $\{\omega_k(t)\} := \{\omega_1, \omega_2, \cdots, \omega_n\}$ is the of central frequencies; ∂_t denotes partial derivative:

Step 2: Solving the variational problem as follows:

$$\mathcal{L}(\{u_k\},\{\omega_k\},\lambda) := \alpha \sum_{k=1}^K \left\| \partial_t \left[\left(\delta(t) + \frac{j}{\pi t}\right) u_k(t)\right] e^{-jw_k^t}\right\|_2^2 + \left\|y(t) - \sum_k^K u_k(t)\right\|_2^2 + \langle \lambda(t), y(t) - \sum_k^K u_k(t)\rangle \tag{29}$$

Where α is the quadratic penalty factor; $\mathcal{L}$ is a Lagrangian augmentation term, and $\lambda(t)$ is the Lagrange multiplier. λ ; ω_k and $u_k(\omega)$ are iteratively updated as:

$$u_k^{n+1}(\omega) = \frac{y(\omega) - \sum_{i\neq k}^K u_i(\omega) + \frac{\lambda(\omega)}{2}}{1 + 2\alpha(\omega - \omega_k)^2} \tag{30}$$

$$\omega_k^{n+1} = \frac{\int_0^\infty \omega |u_k(\omega)|^2 d\omega}{\int_0^\infty |u_k(\omega)|^2 d\omega} \tag{31}$$

$$\lambda^{n+1}(\omega) = \lambda^n(\omega) + \eta(y(\omega) - \sum_{k=1}^K u_k^{n+1}(\omega)) \tag{32}$$

Where η denotes the iteration counter.

The stopping or convergence criterion for the iterations of these steps is defined as:

$$\frac{\sum_k \|u_k^{n+1} - u_k^n\|_2^2}{\|u_k^n\|_2^2} < \varepsilon \tag{33}$$

Where ε represents the convergence threshold or tolerance.

Variance Contribution Rate and Periodic Cycles

According to Guo *et al*. (2016); Bai *et al*. (2017); Agbazo *et al*. (2021), the Variance contribution rate (VCR) is determined as:

$$VCR_{IMF_k} = 100 * \frac{\sigma_{IMF_k}^2}{\sum_{k=1}^n \sigma_{IMF_k}^2 + \sigma_{Trend}^2} \tag{34}$$

$$VCR_{Trend} = 100 * \frac{\sigma_{Trend}^2}{\sum_{k=1}^n \sigma_{IMF_k}^2 + \sigma_{Trend}^2} \tag{35}$$

Where the operator $\sigma_{(.)}^2$ denotes variance sign, *IMF* and Trend represent respectively the intrinsic mode function and the nonlinear trend.

Furthermore, according to Wu and Huang (2004; 2005) the mean period (T_k) of the k^{th} *IMF* is estimated through:

$$T_k = \frac{L}{NP_k} \quad (36)$$

Where L represents the size of *IMF* time series and where NP_k represents the number of local maxima in IMF set.

Performance Evaluation Criteria of Decomposition Techniques

We have used four statistical metrics:

(a) Root Mean Square Error (RMSE) (Gentilucci *et al*., 2019)
(b) Mean Absolute Error (MAE) (Wang and Lu, 2018)
(c) Mean Square Error (MSE) (Luo *et al*., 2022)
(d) Statistic of Kolmogorov-Smirnov (DKS) (Wilks, 2006) to identify the best rainfall decomposition techniques between VMD, EEMD, CEEMD, CEEMDAN and ICEEMDAN for each region. Rainfall data reconstruction was performed by summing IMF components and the overall trend component obtained by each technique. RMSE, MAE and MSE indicate the magnitude of errors between reconstructed and observed rainfall. RMSE, MAE, MSE values are 0, for the best reconstruction accuracy technique

The mathematical expressions of RMSE, MSE and MAE are (Gentilucci *et al*., 2019; Wang and Lu, 2018; Luo *et al*., 2022):

$$RMSE = \left(\frac{1}{N}\sum_{i=1}^{N}(P_{rec}(i) - P_{obs}(i))^2\right)^{1/2} \quad (37)$$

$$MAE = \frac{1}{N}\sum_{i=1}^{N}|P_{rec}(i) - P_{obs}(i)| \quad (38)$$

$$MSE = \frac{1}{N}\sum_{i=1}^{N}(P_{rec}(i) - P_{obs}(i))^2 \quad (39)$$

P_{rec} and P_{obs} are reconstructed and observed rainfall set, respectively; N is the length.

According to Wilks (2006), the mathematical expression of DKS is:

$$DKS = sup_x|F_a(x) - F_b(x)| \quad (40)$$

Where $F_a(x)$ and $F_b(x)$ represent respectively cumulative distribution functions of dataset A and B; sup_x stands for supremum.

Results and Discussion

Figure 2 displays the boxplot of the error made during the decomposition of the series observed by the ICEEMDAN, CEEMDAN, CEEMD, EEMD and VMD techniques. It can be noted that, except for EEMD and VMD techniques, the minimum, median, 25th and 75th percentiles and the maximum values of the error are close to zero in all the studied stations. Thus, among the studied techniques, the reconstructed rainfall data obtained from EEMD and VMD techniques present a huge error compared to the observed rainfall data in all the studied stations. However, the error with VMD is larger than EEMD ones, and the error with EEMD technique is smallest for Nzérékoré and largest for Conakry. Among the studied techniques, VMD is not suitable.

These findings demonstrate that compared to EEMD and VMD, CEEMD, CEEMDAN and ICEEMDAN techniques are systematically more adapted than EEMD and VMD for monthly rainfall decomposition in Guinea.

Figures 3, 4 and 5 present the performances of the decomposition techniques. It is evident from these figures that among all the studied techniques, VMD and EEMD have the largest RMSE, MAE and MSE values at all the studied stations, indicating that EEMD and VMD techniques, especially VMD is not suitable for decomposing monthly rainfall into a limited number of oscillating components, confirming the above results. Furthermore, according to the comparison between the ICEEMDAN, CEEMDAN and CEEMD techniques, it is noted that the CEEMD technique consistently demonstrated higher RMSE, MAE and MSE across all stations, which means that CEEMD is less suitable. On comparing the RMSE, MSE, and MAE values of ICEEMDAN and CEEMDAN techniques, it is observed that the two techniques are relatively close to one another.

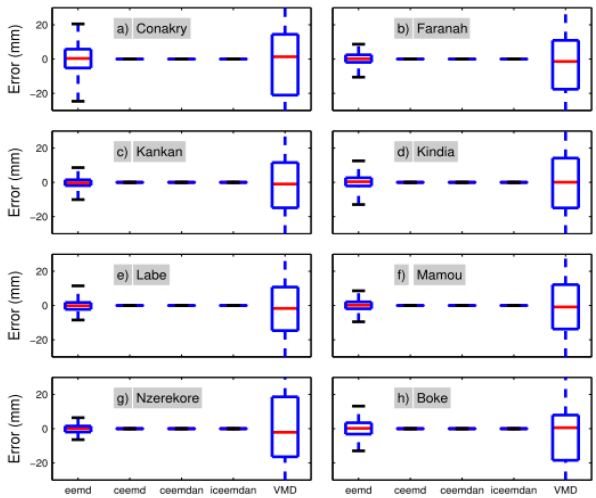

Fig. 2: Box plot of the difference between the observed Rainfall data and the reconstructed rainfall data for ICEEMDAN, CEEMDAN, CEEMD, EEMD and VMD techniques

DOI: 10.3844/ajassp.2025.47.58

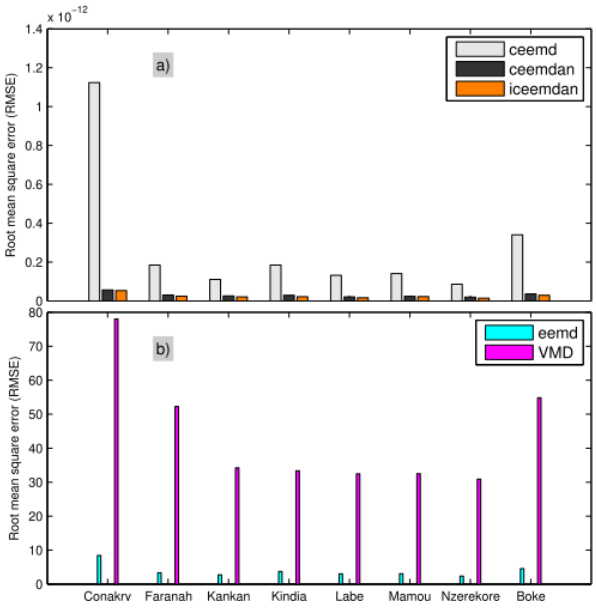

Fig. 3: Root mean square error (rmse) for the reconstruction accuracy of rainfall data using ICEEMDAN, CEEMDAN, CEEMD, EEMD and VMD techniques

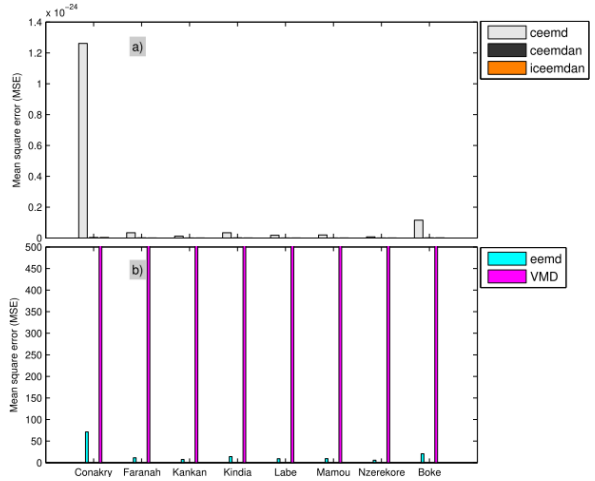

Fig. 4: Mean absolute error (mse) for the reconstruction accuracy of rainfall data using ICEEMDAN, CEEMDAN, CEEMD, EEMD and VMD techniques

Therefore, based on the RMSE, MSE and MAE criteria, it seems that these two techniques exhibit comparable effectiveness for decomposing monthly rainfall and at this step, it is arduous to distinguish the most appropriate technique between them for the studied stations.

The computed values of the Kolmogorov-Smirnov statistic (DKS) for each technique are presented in Figure 6. ICEEMDAN and CEEMDAN techniques have lower DKS values than the CEEMD and EEMD, suggesting and confirming that ICEEMDAN and CEEMDAN perform better than the other two techniques. However, they exhibited varying degrees of effectiveness across the studied stations. ICEEMDAN quasi-systematically shows lower DKS value compared to CEEMDAN in all the studied stations, except for Faranah and Nzérékoré. Therefore, ICEEMDAN is the suitable technique for decomposing monthly rainfall into a limited number of oscillating components in most of the studied stations, while CEEMDAN decomposing performance is significantly better than ICEEMDAN for Faranah and Nzérékoré.

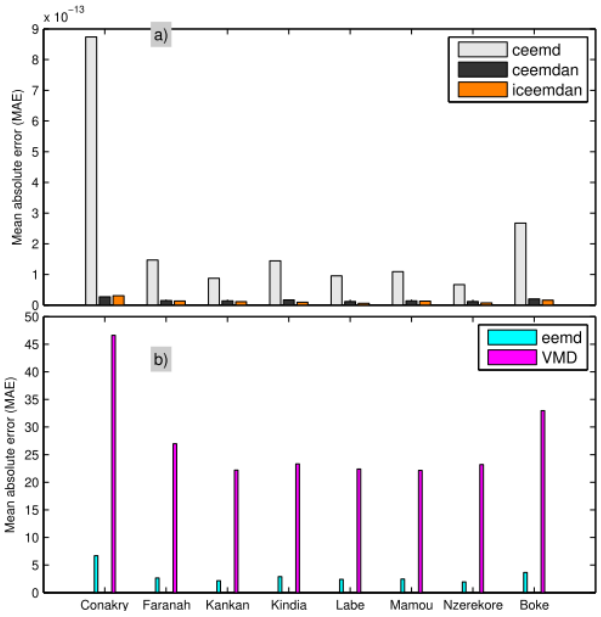

Fig. 5: Mean Square Error (MAE) for the Reconstruction Accuracy of Rainfall Data Using ICEEMDAN, CEEMDAN, CEEMD, EEMD and VMD Techniques

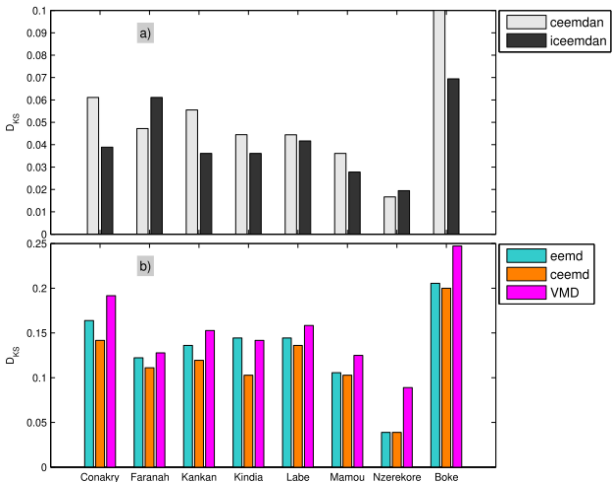

Fig. 6: Spatial Distribution of DKS Statistic Between the Observed and Reconstructed Rainfall Data Using ICEEMDAN, CEEMDAN, CEEMD and EEMD Techniques

DOI: 10.3844/ajassp.2025.47.58

Figure 7 presents the Variance Contribution Rate (VCR), which evaluates the contribution of each IMF to the monthly rainfall variability. The results show that ICEEMDAN decomposes the monthly rainfall time series into six (6) IMF components (IMF1-6) and one trend component at most studied stations for 1991 to 2020, except for Kindia and Labé, where the series is decomposed into five IMF components (IMF1-5) and one trend component. This finding indicates that the variability in monthly rainfall time series is less complex for Kindia and Labé compared to the remaining stations. The underlying reasons for this difference were not investigated.

The variance rate indicates that, at most of the studied stations, except, for Kindia, Labé and Nzérékoré, IMF6 emerged as the dominant component, contributing 60 to 80% of the overall variability in monthly rainfall time series depending on the stations. IMF6 was followed by IMF1, with a contribution rate of 8 to 15% depending on the stations. However, for Kindia, Labé and Nzérékoré, the overall trend component contributes the most for about 40% to 80%, indicating a nonlinear change in the monthly rainfall from 1991-2020. It is followed by IMF1 and IMF5 which contributes for 10% to 20 and 5 to 10% respectively. This result implies that at these stations, the overall trend component represents a significant portion of the monthly rainfall time series variability, suggesting that these stations may be more impacted by climate change effects.

Figure 8 illustrates the periodic cycles of the monthly rainfall components. The results indicate that inter-month scales, inter-annual scales, inter-decadal scales, and multi-decadal scales characterized changes in monthly rainfall during the 1991-2020 period, at all of the studied stations. By combining these findings with those related to the contribution of the IMF components (Figure 7), it can be deduced that, except, for Kindia, Labé and Nzérékoré, inter-decadal, the inter-monthly and inter-annual fluctuations are the primary drivers of monthly rainfall time series variability depending on the station.

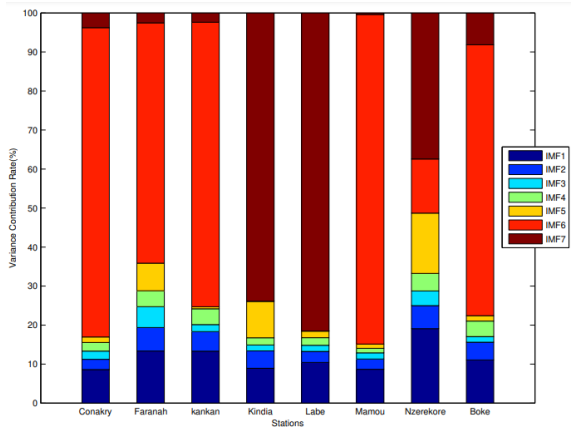

Fig. 7: Variance Contribution Rate (VCR) of IMFs and Trend Component Extracted Using ICEEMDAN Technique

Figure 9 presents the long-term trends extracted. The ICEEMDAN results clearly show that the overall trend in the monthly rainfall time series during the 1991-2020 period for all of the studied stations is nonlinear. Thus, the use of standard trend identification techniques, such as the conventional linear regression technique, that assume a linear fit to the overall trend of rainfall monthly time series could lead to inaccurate interpretations in all of the studied stations.

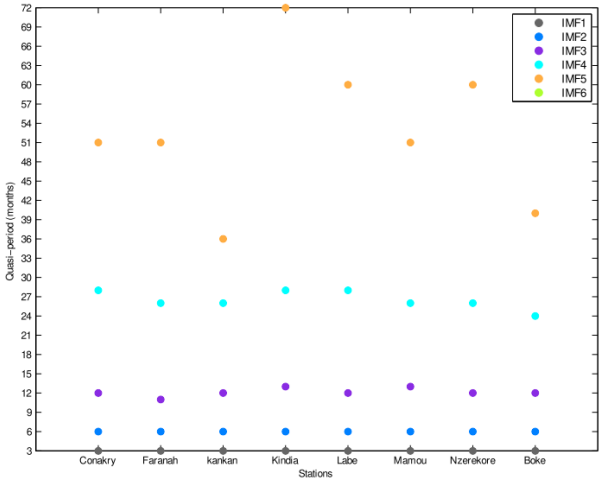

Fig. 8: Mean Period of IMFs Extracted Using the ICEEMDAN Technique

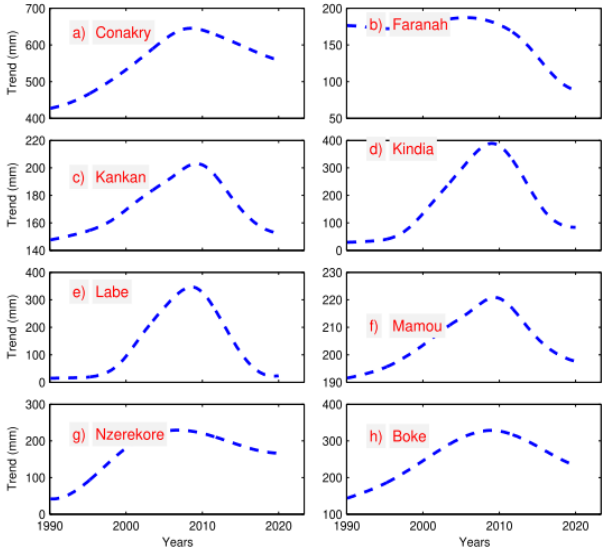

Fig. 9: Intrinsic long-term trends of the rainfall variation obtained from the ICEEMDAN technique during 1991-2020 period in Guinea

The nonlinear trends revealed by ICEEMDAN technique have a parabolic shape with a downward concavity, with maximum values observed around 2010. For all of the stations, the nonlinear trend in the monthly

rainfall time series during the 1991-2020 period exhibits an increasing-decreasing pattern. This trend morphology consists of two distinct phases: The first phase (1991-2010) is the most humid, characterized by a slightly increasing trend in monthly rainfall time series.

The second zone (2010-2020) is the driest or less humid compared to the first ones, marked by a rainfall deficit and characterized by a decreasing trend. Qualitatively, these findings align with results reported in West African countries, such as Burkina-Faso (Yanogo and Yaméogo, 2023). Overall, the monthly rainfall in Guinea for 1991-2020 has a nonlinear change, increases before the late 2010s and decreases after the late 2010s.

Thus, the morphology of the nonlinear trend obtained using ICEEMDAN at the stations aligns with previous research conducted in different West African regions. These studies, identified shift in rainfall trends around 2010s, with a positive trend 1990 and 2010, during the 1982-2013 period (Bodian, 2014; Descroix *et al*., 2015; Vischel *et al*., 2015; Tano *et al*., 2023; Yanogo and Yaméogo, 2023). Consequently, trend detection using ICEEMDAN techniques presents a major advancement over linear trend detection and is strongly recommended.

Overall, two key reasons confirm the capability of the ICEEMDAN technique in detecting and analyzing the nonlinear trend in the studied region: Its ability to explain past results known in the literature through nonlinear trend morphology and the coincidence of past results with those revealed by the nonlinear trend pattern.

The nonlinear trend detected in the monthly rainfall time series in Guinea aligns with previous studies (Xue *et al*., 2013; Duan *et al*., 2019; Guan *et al*., 2022), which identified complex nonlinear changes accompanied by periodic variability in precipitation data in other parts of the world.

Conclusion

The performances of five most popular decomposition techniques in multiscale decomposing of monthly rainfall datasets across Guinea geographical regions during 1991-2020 period were presented in this study. The techniques were tested against four evaluation criteria. ICEEMDAN and CEEMDAN fulfilled three of the evaluation criteria (RMSE, MAE, and MSE) in all of the studied stations. Among the considered techniques, it showed the lowest RMSE, MAE and MSE, which are close to zero over ICEEMDAN and CEEMDAN techniques. Thus, ICEEMDAN and CEEMDAN outperformed other techniques. However, based on the RMSE, MSE and MAE criteria, ICEEMDAN and CEEMDAN showed similar performance for decomposing monthly rainfall in studied stations. Considering DKS values, ICEEMDAN outperformed CEEMDAN in most stations. However, CEEMDAN performs ICEEMDAN in Faranah and Nzérékoré. So, among the considered stations, ICEEMDAN emerged as the most efficient and suggested for decomposing monthly rainfall time series into a limited number of oscillating components without the need for predetermined basis functions in most of the studied stations, while CEEMDAN is recommended for Faranah and Nzérékoré ones. Between 1991 and 2020, the monthly rainfall time series exhibited significant long-term nonlinear trends at nearly all stations studied, highlighting that linear trend techniques can lead to wrong conclusions about the impact of climate change. The nonlinear trends in monthly rainfall are characterized by increasing-decreasing trends, reflecting notable climatic shifts around the 2010s.

These findings highlight our understanding of monthly rainfall trends, crucial for designing and implementing effective climate change resilience strategies in Guinea. These main results also have important implications for improving monthly rainfall forecasting with machine learning approaches in Guinea, which will be our future research topic.

Acknowledgment

We extend our thanks to the Guinean National Meteorological Directorate for providing datasets. We also thank the reviewers for their contribution to the quality of this paper.

Funding Information

This scientific work received no funding.

Author's Contributions

All authors equally contributed in this work.

Ethics

Compliance with ethical standards.

References

Adamowski, J., & Sun, K. (2010). Development of a coupled wavelet transform and neural network method for flow forecasting of non-perennial rivers in semi-arid watersheds. *Journal of Hydrology*, *390*(1–2), 85–91. https://doi.org/10.1016/j.jhydrol.2010.06.033

Adarsh, S., & Reddy, M. J. (2021). *Multi-scale Spectral Analysis in Hydrology: From Theory to Practice (1sted.) CRCPress*. https://doi.org/10.1201/9781003108351

Adarsh, S., & Reddy, M. J. (2018). Multiscale characterization and prediction of monsoon rainfall in India using Hilbert–Huang transform and time-dependent intrinsic correlation analysis. *Meteorology and Atmospheric Physics*, *130*(6), 667–688. https://doi.org/10.1007/s00703-017-0545-6

Agbazo, M. N., N'Gobi, G. K., Alamou, E., Kounouhewa, B., & Afouda, A. (2021). Assessing Nonlinear Dynamics and Trends in Precipitation by Ensemble Empirical Mode Decomposition (EEMD) and Fractal Approach in Benin Republic (West Africa). *Complexity*, *2021*(1), 1–10. https://doi.org/10.1155/2021/3689397

Agbazo, N. M., Tall, M., & Sylla, M. B. (2023). Nonlinear Trend and Multiscale Variability of Dry Spells in Senegal (1951–2010). *Atmosphere*, *14*(9), 1359. https://doi.org/10.3390/atmos14091359

Ali, M., Khan, A., & Rehman, N. ur. (2018). Hybrid multiscale wind speed forecasting based on variational mode decomposition. *International Transactions on Electrical Energy Systems*, *28*(1), e2466. https://doi.org/10.1002/etep.2466

Ali, M., Prasad, R., Xiang, Y., & Yaseen, Z. M. (2020). Complete ensemble empirical mode decomposition hybridized with random forest and kernel ridge regression model for monthly rainfall forecasts. *Journal of Hydrology*, *584*, 124647. https://doi.org/10.1016/j.jhydrol.2020.124647

Antico, A., Schlotthauer, G., & Torres, M. E. (2014). Analysis of hydroclimatic variability and trends using a novel empirical mode decomposition: Application to the Paraná River Basin. *Journal of Geophysical Research: Atmospheres*, *119*(3), 1218–1233. https://doi.org/10.1002/2013jd020420

Bai, L., Liu, Z., Chen, Z., & Xu, J. (2017). Runoff nonlinear variation and responses to climate fluctuation in the headwater region of the Kaidu River. *Resour. Sci*, *39*(8), 1511–1521. https://doi.org/10.18402/resci.2017.08.08

Bodian, A. (2014). Caractérisation de la variabilité temporelle récente des précipitations annuelles au Sénégal (Afrique de l'Ouest). *Physio-Géo*, *8*, 297–312. https://doi.org/10.4000/physio-geo.4243

Colominas, M. A., Colominas, G., Torres, M. E., & Flandrin, P. (2012). NOISE-ASSISTED EMD METHODS IN ACTION. *Advances in Adaptive Data Analysis*, *04*(04), 1250025. https://doi.org/10.1142/s1793536912500252

Colominas, M. A., Schlotthauer, G., & Torres, M. E. (2014). Improved complete ensemble EMD: A suitable tool for biomedical signal processing. *Biomedical Signal Processing and Control*, *14*, 19–29. https://doi.org/10.1016/j.bspc.2014.06.009

Descroix, L., Diongue Niang, A., Panthou, G., Bodian, A., Sane, Y., Dacosta, H., Malam Abdou, M., Vandervaere, J.-P., & Quantin, G. (2015). Évolution récente de la pluviométrie en Afrique de l'ouest à travers deux régions : la Sénégambie et le bassin du Niger moyen. *Climatologie*, *12*, 25–43. https://doi.org/10.4267/climatologie.1105

Danandeh, A. M. (2021). Seasonal rainfall hindcasting using ensemble multi-stage genetic programming. *Theoretical and Applied Climatology*, *143*(1–2), 461–472. https://doi.org/10.1007/s00704-020-03438-3

Dragomiretskiy, K., & Zosso, D. (2014). Variational Mode Decomposition. *IEEE Transactions on Signal Processing*, *62*(3), 531–544. https://doi.org/10.1109/tsp.2013.2288675

Duan, Z., Chen, Q., Chen, C., Liu, J., Gao, H., Song, X., & Wei, M. (2019). Spatiotemporal analysis of nonlinear trends in precipitation over Germany during 1951–2013 from multiple observation-based gridded products. *International Journal of Climatology*, *39*(4), 2120–2135. https://doi.org/10.1002/joc.5939

Gentilucci, M., Materazzi, M., Pambianchi, G., Burt, P., & Guerriero, G. (2019). Assessment of Variations in the Temperature-Rainfall Trend in the Province of Macerata (Central Italy), Comparing the Last Three Climatological Standard Normals (1961–1990; 1971–2000; 1981–2010) for Biosustainability Studies. *Environmental Processes*, *6*(2), 391–412. https://doi.org/10.1007/s40710-019-00369-8

Guan, X., Yao, J., & Schneider, C. (2022). Variability of the precipitation over the Tianshan Mountains, Central Asia. Part I: Linear and nonlinear trends of the annual and seasonal precipitation. *International Journal of Climatology*, *42*(1), 118–138. https://doi.org/10.1002/joc.7235

Guo, B., Chen, Z., Guo, J., Liu, F., Chen, C., & Liu, K. (2016). Analysis of the Nonlinear Trends and Non-Stationary Oscillations of Regional Precipitation in Xinjiang, Northwestern China, Using Ensemble Empirical Mode Decomposition. *International Journal of Environmental Research and Public Health*, *13*(3), 345. https://doi.org/10.3390/ijerph13030345

Guinea, CRP. (2018). *Climate Risk Profile: Country risk profile.*

Huang, C., Li, Q., Xie, Y., & Peng, J. (2022). Prediction of summer precipitation in Hunan based on machine learning. *Trans. Atmos. Sci*, *45*(2), 191–202.

Huang, N. E., Shen, Z., Long, S. R., Wu, M. C., Shih, H. H., Zheng, Q., Yen, N.-C., Tung, C. C., & Liu, H. H. (1998). The empirical mode decomposition and the Hilbert spectrum for nonlinear and non-stationary time series analysis. *Proceedings of the Royal Society of London. Series A: Mathematical, Physical and Engineering Sciences*, *454*(1971), 903–995. https://doi.org/10.1098/rspa.1998.0193

Kante, I.K., Saïdou, M. S., Daouda, B., Idrissa, D., & Ibrahima, D. (2019). Seasonal variability of rainfall and thunderstorm in Guinea over the period 1981 to 2010. *African Journal of Environmental Science and Technology*, *13*(9), 324–341. https://doi.org/10.5897/ajest2019.2684

Kante, I. K., Sall, S. M., Badiane, D., Diouf, I., Dieng, A. L., Diaby, I., & Guichard, F. (2020). Analysis of Rainfall Dynamics in Conakry, Republic of Guinea. *Atmospheric and Climate Sciences*, *10*(01), 1–20. https://doi.org/10.4236/acs.2020.101001

Khan, Md. M. H., Muhammad, N. S., & El-Shafie, A. (2020). Wavelet based hybrid ANN-ARIMA models for meteorological drought forecasting. *Journal of Hydrology*, *590*, 125380. https://doi.org/10.1016/j.jhydrol.2020.125380

Iyengar, R. N., & Raghu Kanth, S. T. G. (2005). Intrinsic mode functions and a strategy for forecasting Indian monsoon rainfall. *Meteorology and Atmospheric Physics*, *90*(1–2), 17–36. https://doi.org/10.1007/s00703-004-0089-4

Jiang, X. (2023). A combined monthly precipitation prediction method based on CEEMD and improved LSTM. *PLOS ONE*, *18*(7), e0288211. https://doi.org/10.1371/journal.pone.0288211

Jiao, X., & He, Z. (2024). A novel coupled rainfall prediction model based on stepwise decomposition technique. *Scientific Reports*, *14*(1), 10853. https://doi.org/10.1038/s41598-024-61855-0

Johny, K., Pai, M. L., & Adarsh, S. (2020). Adaptive EEMD-ANN hybrid model for Indian summer monsoon rainfall forecasting. *Theoretical and Applied Climatology*, *141*(1–2), 1–17. https://doi.org/10.1007/s00704-020-03177-5

Li, C., Wang, X., Hu, Y., Yan, Y., Jin, H., & Shang, G. (2023). Forecasting shipping index using CEEMD-PSO-BiLSTM model. *PLOS ONE*, *18*(2), e0280504. https://doi.org/10.1371/journal.pone.0280504

Ling, M., Xiao, Liying, Jia, Wang, Pinggen, Wang, Yin, Xiang, Kai, Cai, & Gaotang. (2023). Daily precipitation prediction based on SVM-CEEMDAN-BiLSTM Mode. *Pearl River*, *44*(09), 61–68.

Luo, S., Zhang, M., Nie, Y., Jia, X., Cao, R., Zhu, M., & Li, X. (2022). Forecasting of monthly precipitation based on ensemble empirical mode decomposition and Bayesian model averaging. *Frontiers in Earth Science*, *10*, 1–13. https://doi.org/10.3389/feart.2022.926067

Pati, Y. C., Rezaiifar, R., & Krishnaprasad, P. S. (1993). Orthogonal matching pursuit: recursive function approximation with applications to wavelet decomposition. *Proceedings of 27th Asilomar Conference on Signals, Systems and Computers*, 40–44. https://doi.org/10.1109/acssc.1993.342465

Poongadan, S., & Lineesh, M. C. (2024). Non-linear Time Series Prediction using Improved CEEMDAN, SVD and LSTM. *Neural Processing Letters*, *56*(3), 164. https://doi.org/10.1007/s11063-024-11622-z

Rezaiy, R., & Shabri, A. (2024). Enhancing drought prediction precision with EEMD-ARIMA modeling based on standardized precipitation index. *Water Science & Technology*, *89*(3), 745–770. https://doi.org/10.2166/wst.2024.028

Sánchez-Monedero, J., Salcedo-Sanz, S., Gutiérrez, P. A., Casanova-Mateo, C., & Hervás-Martínez, C. (2014). Simultaneous modelling of rainfall occurrence and amount using a hierarchical nominal–ordinal support vector classifier. *Engineering Applications of Artificial Intelligence*, *34*, 199–207. https://doi.org/10.1016/j.engappai.2014.05.016

Seo, Y., Kim, S., & Singh, V. P. (2015). Estimating Spatial Precipitation Using Regression Kriging and Artificial Neural Network Residual Kriging (RKNNRK) Hybrid Approach. *Water Resources Management*, *29*(7), 2189–2204. https://doi.org/10.1007/s11269-015-0935-9

Tan, Q.-F., Lei, X.-H., Wang, X., Wang, H., Wen, X., Ji, Y., & Kang, A.-Q. (2018). An adaptive middle and long-term runoff forecast model using EEMD-ANN hybrid approach. *Journal of Hydrology*, *567*, 767–780. https://doi.org/10.1016/j.jhydrol.2018.01.015

Tano, A. R., Bouo, F.-X. D. B., Kouamé, J. K., Tchétché, Y., Zézé, S. D., & Ouattara, B. (2023). Rainfall Variability and Trends in West Africa. *Atmospheric and Climate Sciences*, *13*(01), 72–83. https://doi.org/10.4236/acs.2023.131006

Torres, M. E., Colominas, M. A., Schlotthauer, G., & Flandrin, P. (2011). A complete ensemble empirical mode decomposition with adaptive noise. In *2011 IEEE International Conference on Acoustics, Speech and Signal Processing (ICASSP)* (pp. 4144–4147). https://doi.org/10.1109/icassp.2011.5947265

USAID. (2018). Guinea: Environment and Global Climate Change. *International Data and Economic Analysis (IDEA) Website*.

Vischel, T., Lebel, T., Panthou, G., Quantin, G., Rossi, A., & Martinet, M. (2015). Le retour d'une période humide au Sahel? In B. Sultan, R. Lalou, M. A. Sanni, A. Oumarou, & M. A. Soumaré (Eds.), *IRD Éditions / OpenEdition Books* (pp. 43–60). IRD Éditions. https://doi.org/10.4000/books.irdeditions.8937

Wang, C., Jia, Z., Yin, Z., Liu, F., Lu, G., & Zheng, J. (2021). Improving the Accuracy of Subseasonal Forecasting of China Precipitation With a Machine Learning Approach. In *Frontiers in Earth Science* (Vol. 9, pp. 1–15). https://doi.org/10.3389/feart.2021.659310

Wang, W., & Lu, Y. (2018). Analysis of the Mean Absolute Error (MAE) and the Root Mean Square Error (RMSE) in Assessing Rounding Model. In *IOP Conference Series: Materials Science and Engineering* (Vol. 324, p. 012049). https://doi.org/10.1088/1757-899x/324/1/012049

Wani, O. A., Mahdi, S. S., Yeasin, Md., Kumar, S. S., Gagnon, A. S., Danish, F., Al-Ansari, N., El-Hendawy, S., & Mattar, M. A. (2024). Predicting rainfall using machine learning, deep learning, and time series models across an altitudinal gradient in the North-Western Himalayas. In *Scientific Reports* (Vol. 14, Issue 1, p. 27876). https://doi.org/10.1038/s41598-024-77687-x

Wilks, D. S. (2006). *Statistical methods in the atmospheric sciences*. *59*.

Wu, C. L., Chau, K. W., & Li, Y. S. (2009a). Methods to improve neural network performance in daily flows prediction. In *Journal of Hydrology* (Vol. 372, Issues 1–4, pp. 80–93). https://doi.org/10.1016/j.jhydrol.2009.03.038

Wu, C. L., Chau, K. W., & Li, Y. S. (2009b). Predicting monthly streamflow using data-driven models coupled with data-preprocessing techniques. *Water Resources Research*, *45*(8), W08432. https://doi.org/10.1029/2007wr006737

Wu, H. (2009). Ensemble Empirical Mode Decomposition: A Noise-Assisted Data Analysis Method. *Advances in Adaptive Data Analysis*, *01*(01), 1–41. https://doi.org/10.1142/s1793536909000047

Wu, Z., & Huang, N. E. (2004). A study of the characteristics of white noise using the empirical mode decomposition method. In *Proceedings of the Royal Society of London. Series A: Mathematical, Physical and Engineering Sciences* (Vol. 460, Issue 2046, pp. 1597–1611). https://doi.org/10.1098/rspa.2003.1221

Wu, Z., Huang, N. E., & Chen, X. (2009c). The Multi-Dimensional Ensemble Empirical Mode Decomposition Method. In *Advances in Adaptive Data Analysis* (Vol. 01, Issue 03, pp. 339–372). https://doi.org/10.1142/s1793536909000187

Word Bank. (2016). Databank Country Profiles-Guinea. *World Bank DataBank, International Data and Economic Analysis (IDEA)*.

Word Bank. (2017). The World Bank in Guinea. *World Bank Official Website*.

Xu, D., Wang, Y., & Wanng, W. (2022). Monthly precipitation prediction model based on VMD-TCN. *J. China Hydrol*, *2*(02), 13–18. https://doi.org/10.19797/j.cnki.1000-0852.20210101

Xue, C.F., Wei, H., Jun-Hu, Z., & Shi-Gong, W. (2013). The application of ensemble empirical mode decomposition method in multiscale analysis of region precipitation and its response to the climate change. *Acta Physica Sinica*, *62*(10), 109203. https://doi.org/10.7498/aps.62.109203

Yang, K., Wang, Y., & Duan, G. (2024). Displacement Prediction Method for Rainfall-Induced Landslide Using Improved Completely Adaptive Noise Ensemble Empirical Mode Decomposition, Singular Spectrum Analysis, and Long Short-Term Memory on Time Series Data. *Water*, *16*(15), 2111. https://doi.org/10.3390/w16152111

Yang, Q., Qin, L., Gao, P., & Zhang, R. (2021). Annual precipitation prediction in the economic zone of the northern slope of Tianshan Mountain based on EEMD-LSTM model. *Arid Zone Research*, *38*(05), 1235–1243. https://doi.org/10.13866/j.azr.2021.05.05

Yanogo, I. P., & Yaméogo, J. (2023). Recent rainfall trends between 1990 and 2020: Contrasting characteristics between two climate zones in Burkina Faso (West Africa). *Glasnik Srpskog Geografskog Drustva*, *103*(1), 87–106. https://doi.org/10.2298/gsgd2301087y

Zhang, X., Cheng, W., Zhang, Y., Zhu, J., & Ren, H. (2025). A combined model based on secondary decomposition and the optimized support vector machine algorithm for regional rainfall forecasting. *Journal of Water and Climate Change*, *16*(2), 474–492. https://doi.org/10.2166/wcc.2025.512

Zhang, X., Yin, Q., Liu, F., Li, H., & Qi, Y. (2023). Comparative study of rainfall prediction based on different decomposition methods of VMD. *Scientific Reports*, *13*(1), 20127. https://doi.org/10.1038/s41598-023-47416-x

Zhang, X., Zhao, D., Wang, T., Wu, X., & Duan, B. (2022). A novel rainfall prediction model based on CEEMDAN-PSO-ELM coupled model. In *Water Supply* (Vol. 22, Issue 4, pp. 4531–4543). https://doi.org/10.2166/ws.2022.115

Zhou, Y., Liang, Z., Li, B., Huang, Y., Wang, K., & Hu, Y. (2021). Seamless Integration of Rainfall Spatial Variability and a Conceptual Hydrological Model. *Sustainability*, *13*(6), 3588. https://doi.org/10.3390/su13063588